Effective Bandgap Lowering of CdS Deposited by Successive Ionic Layer Adsorption and Reaction

ARTICLE *in* THE JOURNAL OF PHYSICAL CHEMISTRY C · JANUARY 2013

Impact Factor: 4.77 · DOI: 10.1021/jp3105453

THE JOURNAL OF PHYSICAL CHEMISTRY C

Article

pubs.acs.org/JPCC

Effective Bandgap Lowering of CdS Deposited by Successive Ionic Layer Adsorption and Reaction

Elena Rabinovich and Gary Hodes*

Department of Materials and Interfaces, Weizmann Institute of Science, Rehovot 76100, Israel

Supporting Information

ABSTRACT: SILAR (successive ionic layer adsorption and reaction) is a solution process used to deposit semiconductors that has become very common in the past few years as a method to deposit light absorbers in nanoporous solar cells. Films of CdS (possibly the most commonly deposited semiconductor using this method) often show an anomalously low apparent bandgap (lowered by as much as 10%) for sufficiently thick films, although this effect has been ignored in most cases. Here, we study this bandgap lowering and show that it is due not so much to a lower bandgap but rather to a particularly long absorption tail that extends far into the red, and that is amplified by a large optical thickness in the high surface area nanoporous films. The tail is presumably due to as yet unidentified, but probably bulk defects in the CdS. Additionally, the absorption coefficient of the SILAR CdS was nearly twice as high as normal values.

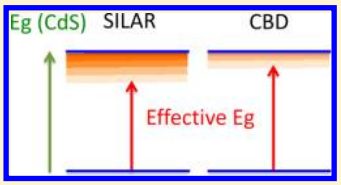

INTRODUCTION

SILAR (successive ionic layer adsorption and reaction) is a solution process for deposition of thin films of various materials, mostly used for semiconductors. The process is a solution analogue of atomic layer deposition (ALD) where the films are built up atom-by-atom using a self-limiting reaction as in ALD, but from solution, usually aqueous. Probably the most common example of SILAR is CdS deposition, where a substrate is sequentially immersed in a solution of Cd^{2+} and then S^{2-}, the sample being rinsed between each dip. The purpose of the rinse step is to remove adsorbed ions except for an adsorbed ionic monolayer plus, presumably, some neutralizing counterions. This adsorbed monolayer then reacts chemically with the ion of opposite charge during the second dip forming (ideally) one molecular monolayer of CdS. The process is then repeated until the required thickness is obtained. The method was introduced by Nicolau[1] for CdS and ZnS and Ristov et al. for Cu_2O (in this variation, no rinsing was carried out between dips, so film formation is much faster and less controlled),[2] and since then has been extended to many semiconductors and solid solutions.

Despite the apparent attractiveness of the method, it is only fairly recently that it has become a commonly used method, where it has been very successfully used to deposit the light-absorbing semiconductor in semiconductor-sensitized solar cells (SSSCs). Its use for this purpose was first demonstrated by Weller about 20 years ago,[3,4] but it is mainly in the past 5 years that it has become a mainstream method for SSSCs (see, e.g., Kamat et al., ref 5). Part of the reason for its common use for these cells is that, due to the high surface area of the substrate, usually nanoporous TiO_2 or ZnO, on which the films are deposited, only a small number of layers need be deposited: Deposition of thick layers, requiring many cycles of deposition, is time-consuming, even with an automated deposition system, while for a small number of layers, the method is very simple.

A survey of the literature, most of which deals with CdS, on SSSCs using SILAR to deposit the absorber shows an interesting trend: The optical absorption spectra shift to the red with increasing thickness. While initially this can be explained by decrease in size quantization as the crystal size grows, the red shift continues with increasing film thickness (number of deposition cycles) beyond that expected from the bulk semiconductor, and the resulting apparent bandgap is considerably lower than standard bulk values. Despite the fact that this anomalous absorption has been recorded in many papers, it has very rarely been commented on. The main exception is by Baker and Kamat[6] who noted a red shift up to 50 nm for SILAR CdS on nanoporous TiO_2 beyond the normal CdS bulk bandgap of 2.4 eV (i.e., to ca. 2.19 eV). They refer to similar observations of apparent red shifts of chemically deposited semiconductors (although not specifically SILAR) in the past literature and suggest two possible explanations, which we will discuss later. Ardelan et al.[7] also point out similar red shifts of CdS, referring to the Baker and Kamat paper for explanation. Two recent papers describe similar red shifts of CdS (not SILAR) nanotubes consisting of ca. 4 nm CdS nanoparticles, and made by a solution method involving reaction of S^{2-} with $KCdCl_3$ nanowires[8] and TiO_2 colloids made by a solvothermal method,[9] explaining the red shifts by metal ion−metal ion bonding. These papers will also be treated in more detail in our discussion below.

Here, we describe this red shift for films of CdS deposited by SILAR and provide experimental evidence to elucidate the cause for the phenomenon.

Received: October 24, 2012
Revised: January 3, 2013

   dx.doi.org/10.1021/jp3105453 | J. Phys. Chem. C XXXX, XXX, XXX−XXX

EXPERIMENTAL SECTION

Sample Preparation. Most of the samples of SILAR CdS were deposited on F-doped tin oxide (FTO) glass (Tec 8) coated with a layer of ZnO nanorods. The ZnO was deposited by chemical bath deposition (CBD) as previously described.[10] In brief, the FTO substrates were activated by immersion in a $KMnO_4$ solution to form Mn(O)OH nuclei as a nucleating layer for the ZnO. The ZnO was deposited by CBD from an ethanolamine/ammonia-complexed solution of $Zn(Ac)_2$ at 90 °C for 40 min to form ZnO nanorods of ca. 3 μm in length and ca. 200 nm diameter. The SILAR CdS was deposited on the ZnO using a home-built automatic apparatus. The substrate was successively immersed in 0.14 M Na_2S in 70% MeOH–water; rinsed in 50% MeOH–water (three rinses); immersed in 0.16 M $Cd(Ac)_2$ in 50% MeOH–water; and again rinsed as before. Each immersion was for 30 s. This constituted one SILAR cycle. This was repeated for the required number of cycles. With time, the cadmium and sulfide concentrations in the rinsing solutions increase, leading to less efficient rinsing and formation of particulate CdS. To prevent this, after about every 30 cycles, we treat the samples for a few minutes in a clean rinsing solution in an ultrasonic bath and also change the three rinsing solutions in the deposition process.

In some experiments, for comparison, CdS was deposited by CBD from a modification of a published citrate bath.[11] This bath was used because, unlike many other CdS baths, it did not noticeably etch the ZnO. First, the ZnO was treated with a 0.1 M aqueous Na_2S solution for 10 min at room temperature (1 min for the dense ZnO), which forms a thin ZnS film on the ZnO and promotes homogeneous nucleation of the CdS on the nanorods.[12] This treatment is not necessary for the SILAR deposition because it already incorporates the Na_2S treatment. The CdS bath composition was: 0.025 M $CdCl_2$, 0.2 M $C_6H_5O_7Na_3O_7$ (sodium citrate), 0.05 M KOH, 0.5 mL borate buffer (pH = 10) for every 10 mL of deposition solution, and 0.1 M thiourea. The deposition was carried out at 8 °C (instead of 70 °C as in ref 12, which was found to give a very rapid reaction with deposition mainly on top of the nanorods rather than a homogeneous coating over their entire area). Deposition was carried out from 30 min to 24 h depending on the sample.

In some experiments, substrates of glass microscope slides or FTO glass were also used for the CdS deposition.

CoS counter electrodes for the solar cell measurements were electrochemically deposited on FTO from an aqueous solution of $CoCl_2 \cdot 6H_2O$ (0.36 M) and KSCN (0.2 M). The method is a modification of the method reported by Smith et al.,[13] and electrodeposition conditions were as in this reference except for the different anion of the Co salt, the deposition time (2 min), and the use of separated electrodes (to use the same solution for many depositions, the Pt counter electrode was separated by a glass frit from the working electrode and the solution mixed between depositions because the pH changes close to the electrodes). A solution could be used for more than 30 electrode depositions.

Characterization Methods. Optical transmission and total (diffuse + specular) reflectance spectra were measured on a JASCOV-570 UV–vis–IR spectrophotometer fitted with an integrating sphere. A few spectra used to quantify transparency (specified in the text) were measured without the sphere. The transmission values shown in this paper (T) are all corrected for reflectance (R). We compared two different approximations for this correction:

$$T = 1 - R^2(e^{-\alpha x})/(1 - R)^2(e^{-2-\alpha x}) \quad (1)$$

.

$$T = T_m/(1 - R) \quad (2)$$

Correction 1 is a generally used equation allowing for multiple reflection from different surfaces. Correction 2 is one we have previously found to be most suitable for thin, transparent films, where only reflection from the front surface is considered. We found correction 2 to be best based on two criteria: (a) Use of absorption values calculated by this method, when fed into the external quantum efficiency spectra, gave the most reasonable internal quantum efficiency values near the absorption edge: Both corrections underestimated the true absorption, but correction 2 did so to a lesser degree. (b) The shape of the T spectra in the region where there was no or little absorption was flattest as a function of wavelength (theoretically it should be flat). However, for the purposes of the results shown in this Article, there was no important difference between the two corrections with regard to the conclusions obtained using either method.

In all cases, because there is invariably some light lost in the measurement (e.g., through the sides of the glass substrates), we multiply the corrected T by a factor that brings it to 1 (100%) at a wavelength where absorption is zero (just prior to onset of absorption); that is, we normalize the spectra. We can measure this absorption onset accurately from the photocurrent spectra (discussed in more detail later). Because it is difficult to measure the onset exactly, as there is a very long photocurrent tail and very small photocurrents can be measured out to almost arbitrary long wavelengths at high enough sensitivity, we use a more quantitative measure of onset at the wavelength where the quantum efficiency is 0.1%. Clearly there is still some small absorption at this point; however, it is small enough that we can reasonably consider it as an onset point without the experimental complication of trying to define a true onset (where the photocurrent signal blends into the noise signal) and over a broad region where the signal is so low as to be negligible for our purposes. The error from using this value will be almost negligible when translated into the %T spectra shown below.

Scanning electron microscopy (SEM) characterization was carried out on a Leo Ultra 55 scanning electron microscope, using 2 kV accelerating voltage. Transmission electron microscopy (TEM) imaging was made on a Philips CM120 transmission electron microscope using a 120 kV electron beam.

Phase and crystal size analyses were carried out by X-ray diffraction (XRD) on a Rigaku TTRAXIII diffractometer. The measurements were performed in the Bragg–Brentano (θ–2θ) mode using Cu Kα radiation. Profile fitting and Kα1–Kα2 deconvolution were performed using Jade 9 software (MDI, CA).

XPS measurements were carried out on a Kratos AXIS-HS system using a monocromatized Al Kα X-ray source at 75 W and detection pass energies ranging between 20 and 80 eV.

Cells were assembled using the ZnO/CdS as photoanode and a CoS counter electrode, which were assembled together using a 400 μm thick Surlyn spacer (Surlyn 1702, DuPont). The aqueous polysulfide electrolyte (1 M Na_2S, 1 M S, and 1 M NaOH) was injected into the cell with vacuum assistance through a predrilled hole of ca. 2 mm diameter in the counter

dx.doi.org/10.1021/jp3105453 | J. Phys. Chem. C XXXX, XXX, XXX–XXX

Table 1. CdS Thickness−Local Thickness on Individual ZnO Nanorods[a]

number of SILAR cycles	CdS thickness (nm)	TEM crystal size (nm)	XRD crystal size (nm)	EQE onset (nm)	effective bandgap (nm/eV)	EQE extrap. (nm)	EQE^2 extrap. (nm)
5	4−7	3.3−5 × 7−9		505	473/2.63	465	450
7				558	500/2.49	495	480
10	7−9	4.7−5.5 × 7−9		584	530/2.35	526	510
20	7.5−11	5−7 × 7.5−12		613	550/2.26	550	534
50	14−19		5	646	570/2.18	574	554
100	22−27			646	580/2.14	576	560
140	30−33		6−7	676	590/2.11	600	578
220	42−48			680	595/2.09	605	580
140 (540 °C)	32−40			666	570/2.18	564	542
CBD film	30−35		6	600	520/2.39	535	520

[a]No XRD signal was seen for films of <50 cycles. EQE onset: wavelength at which EQE = 0.1%. Other columns described in the text.

electrode and closed with scotch tape (which was sufficient for the time needed to do these measurements).

Cell quantum efficiency measurements were performed using a setup including a 300 W Xe arc lamp and monochromator (Oriel Cornerstone 1/4 m) together with a standard Si photodiode (Hamamatsu Photonics) for quantum efficiency calibration.

RESULTS AND DISCUSSION

The gradual red shift of the transmission spectra of SILAR CdS on ZnO nanorod films is shown in Figure 1. The spectra are labeled by the number of SILAR cycles. The measured CdS thicknesses (local thickness on the ZnO nanorods) and crystal size information, measured by SEM (Figure S5 in the Supplementary Information), TEM (Figure S1 in the Supporting Information), and XRD for some of the samples, are given in Table 1. A CBD film and an annealed (140 540C) SILAR film are also shown.

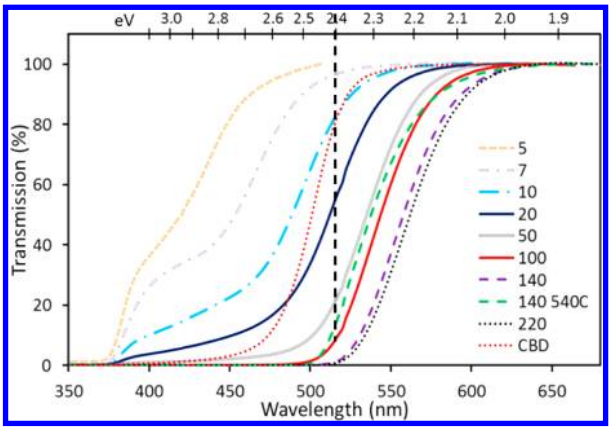

Figure 1. Reflection-corrected and normalized transmission spectra of SILAR films of various number of deposition cycles (given in the figure). The thicknesses of the various layers are given in Table 1. Also shown are a CBD film and an annealed (540 °C in N_2) 140 cycle SILAR film. The vertical broken line shows the room temperature normal bandgap of CdS.

The roughness factor of the ZnO is approximately a factor of 20 (derived later); that is, a local thickness of 10 nm gives an optical thickness of the film of 200 nm. We ignore multiple scattering in the films, which may occur particularly where the intrinsic absorption is low, because we believe it to have at most only a very minor contribution as will be shown later. Looking only at the unannealed SILAR plots for the moment, the increase in optical thickness as the number of cycles increases is clear. Also, the thinnest films, which initially show a strong blue shift, as expected from size quantization, shift to the expected bulk bandgap value of CdS (the vertical dashed line at 2.4 eV) after 10 cycles. However, the curves continue to shift to the red as the number of cycles increases with an eventual estimated effective bandgap (see below) of about 2.1 eV.

Tauc plots $[(\alpha h\nu)^n$ vs $h\nu]$ (Figure S2 in the Supporting Information), with $n = 2$ (for a direct bandgap), can be extrapolated to varying bandgap values, which, while apparently not consistent with a simple visual inspection of the spectra in Figure 1, will later be shown to be fully consistent with these spectra. Figure S2 also shows plots with $n = 0.5$ and 1, from which straight line extrapolations can also be made. We have sometimes found that well-known direct gap semiconductors sometimes give Tauc plots that follow an exponent less than 2.[14,15] However, taking the $n = 2$ extrapolations to be valid, then the bandgaps obtained for the SILAR films range from 2.47 eV for the 10 cycles film to 2.33 eV for the thickest films.

Because of the apparent inconsistency between the calculated bandgap values and the optical spectra, we define an effective bandgap as the intersection between the lines drawn through the sharp drop portions in $\%T$ and the 100% T value. Such an approximation would be normally be expected to be close to the actual bandgap of a direct bandgap material. As will be seen below, these values agree fairly well with values obtained from spectral response data. The effective bandgaps, measured as described above, are given in Table 1.

The literature shows a few examples of anomalous red shifts in spectral response of photocurrent of cells based on SILAR CdS on porous TiO_2 or ZnO, whether recognized or not.[6,7,16−18] What is important is that most of these red shifts appear to be genuine shifts of the response rather than a tail added to the main response, which is common in spectral responses of photoelectrochemical cells (ref 6 is an exception; the extended red response appears to be a strong tail with a sharper normal bandgap response).

Figure 2 shows such spectral responses (shown as external quantum efficiency, EQE) measured for cells made from the samples in Figure 1. The drop in external quantum efficiency with thicker CdS films is a common feature of these cells and can be explained by greater grain boundary recombination as photogenerated electrons have a greater distance on average to travel before being injected into the ZnO.[19] However, our interest in these spectra is not so much in the value of quantum efficiency (although later we do also consider this aspect briefly) but rather in their use in defining absorption/

dx.doi.org/10.1021/jp3105453 | J. Phys. Chem. C XXXX, XXX, XXX−XXX

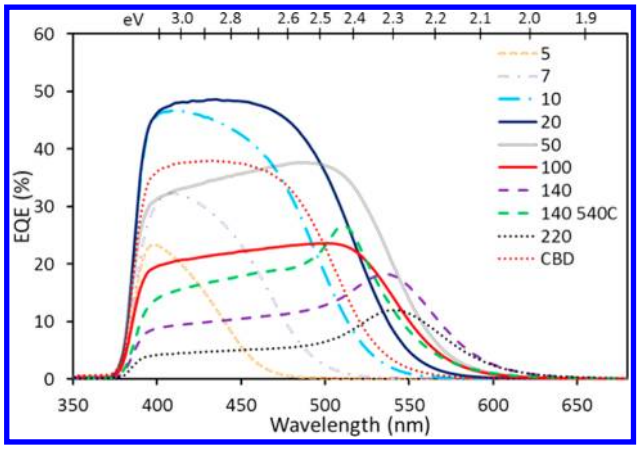

Figure 2. External quantum efficiency (EQE) photoresponse spectra of the samples in Figure 1 in polysulfide electrolyte.

photocurrent onset more accurately than possible from the transmission measurements. Because a spectrophotometer really measures transmission, low values of absorption will not be measured reliably, particularly for scattering films, even after estimations for scattering and reflection losses are made. Photocurrent, on the other hand, can only be generated if light is absorbed. Therefore, onset of photocurrent in the spectral response can be directly correlated with onset of absorption. It is possible to have light absorption that does not lead to photocurrent; however, if photocurrent is measured, then light has been absorbed. As described in the Experimental Section, we define the EQE onset as the wavelength where the EQE = 0.1%, although there is still a small response considerably beyond this (Figure S3 in the Supporting Information shows these EQE tails at very high sensitivity). Table 1 shows these EQE onsets for the films in Figure 1.

Again, we use a qualitative method of estimating an effective bandgap from the spectral responses by extrapolating the roughly linear region of strongly increasing photocurrent to zero current. These values are also shown in Table 1, and for the most part, agree well with those estimated from the optical spectra. Bandgaps can also be calculated from spectral response by extrapolation of the square of the photocurrent (equivalent to EQE^2) to zero photocurrent.[20] However, there are a number of criteria in this calculation (reverse bias, depletion layer controlled, lack of multiple scattering) that are not or probably not fulfilled by the present samples, and we consider it unlikely that all of these criteria are valid for them. However, we also include this analysis in the table (in units of nm): It gives values higher by between 60 and 90 meV than those estimated from either of the other two qualitative methods.

There are many examples in the literature of apparent decreases in bandgap of a photosensitive material caused, for example, by doping. The optical spectra of such samples often show a moderate, possibly even a strong, absorption in the sub-bandgap region. However, quantum efficiency measurements of such samples invariably show either a low QE tail at wavelengths longer than the bandgap of the pure material, or else very low QEs over the whole absorption range.[21−24] In the present case, in contrast, from observation of the optical spectra, there appears to be a genuine red shift of the bandgap with at least moderate values of EQE maintained at photon energies lower than the normal bandgap. (We note that, except for one specific sample, the present films are intentionally not annealed. The EQE of the annealed sample is higher than for the nonannealed one, but this is accompanied by a blue shift of the spectrum.)

Optical effects due to light scattering may be important in explaining the red-shifted spectrum. However, it should be kept in mind that scattering in a totally nonabsorbing film will not lead to any absorption; it can only increase an already existing absorption, although it may do so to an extent that absorption, which in a transparent film was essentially not noticeable, becomes much stronger in the scattering film. We have carried out some experiments correlating the spectra with scattering. However, as we will show later, the increase in surface area resulting in a greater total thickness of absorber is the main factor involved in the red shift, rather than multiple scattering, at least in our samples (multiple scattering could be important in other cases). Therefore, these experiments are described in the Supporting Information.

We next compare the spectra of highly transparent thicker films of CdS, both SILAR and CBD, on FTO glass to remove any effects of scattering and also to find the difference between the CBD film and the SILAR ones of comparable (optical) thickness (Figure 3). The spectrum of the CBD film is blue-

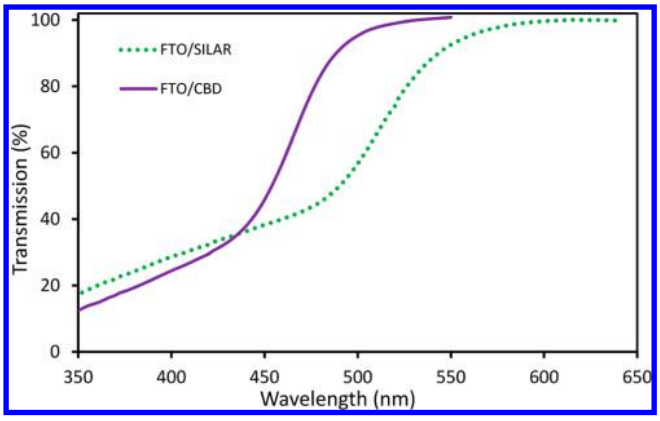

Figure 3. Normalized transmission spectra for 175 cycle CdS layer on FTO/glass (70 nm thick) and a CBD layer (of comparable spectral shape, 160 nm thick) also on FTO glass.

shifted, even compared to "normal" CdS, and we attribute this to size quantization (XRD size ca. 5 nm). Size quantization is common for CBD CdS films deposited from citrate baths, and particularly so because the CBD was carried out at 8 °C. This was found to be a suitable temperature for deposition on ZnO, although it was much slower on FTO: However, we wanted to keep the deposition conditions fixed when comparing deposits on ZnO and on FTO. We also show the EQE spectra of these films (Figure 4). Even ignoring the shifts due to size quantization of the CBD, it is clear, particularly from the higher sensitivity spectra (Figure 4b), that the absorption onset tail of the SILAR film is longer and more gradual than that of the CBD samples. We should note that the measured thickness of the SILAR film on FTO/glass (70 nm for 180 cycles) is nearly twice as thick as for films on ZnO with a comparable number of cycles. We do not know if this is a function of different substrates or a rinsing artifact (although we use three rinses between dips and therefore do not expect such artifacts). In any case, because we use the information from this film on FTO/glass based on its measured thickness, this does not affect our interpretations using this film.

Tauc plots of these transparent, planar films might be expected to be better behaved than the scattering films on ZnO,

dx.doi.org/10.1021/jp3105453 | J. Phys. Chem. C XXXX, XXX, XXX−XXX

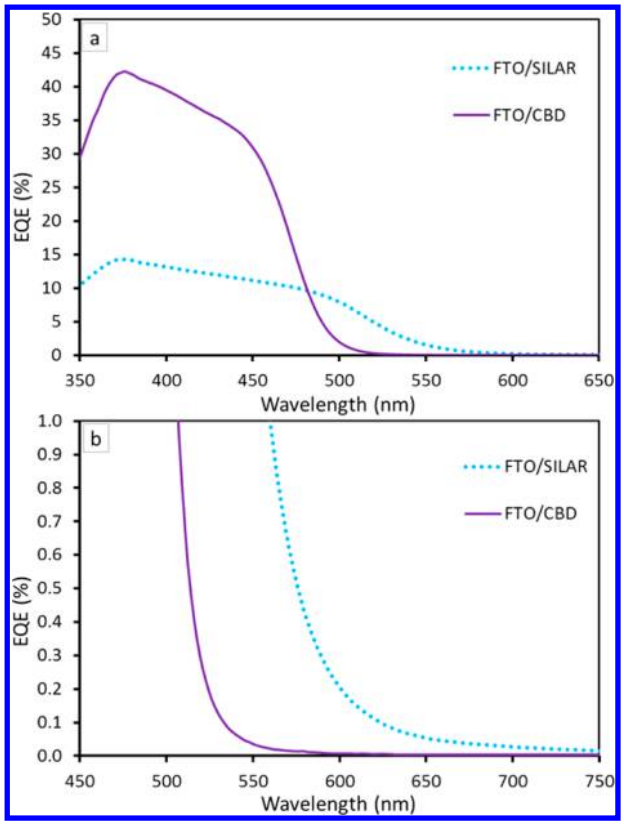

Figure 4. (a) EQE spectral responses of the two planar cells on FTO: 180 cycles SILAR on FTO (SILAR/FTO); CBD on FTO (CBD/FTO). (b) Higher sensitivity spectra in the long wavelength region.

particularly if multiple scattering occurs in the scattering films. Figure S7 shows such plots, again for three different values of n. As for the films on ZnO in Figure S2, both the planar SILAR and the CBD films show regions of linearity for all three values of n. For the moment, we simply note that the SILAR film does extrapolate to a bandgap of nearly 2.4 eV for $n = 2$, as for the thick SILAR films on ZnO.

We can use these data on planar, nonscattering films to calculate the expected spectra of (optically) thicker films, such as those deposited on the nanoporous ZnO, but ignoring scattering effects using the equation:

$$\ln(T) = -\alpha t$$

where T is the transmission, α is the absorption coefficient, and t is the total CdS thickness. Because we are particularly interested in the tail region where transmission is high, and because measurement of absorption from $\%T$ spectra in this region is unreliable, and becomes increasingly less reliable with increasing wavelength, where scattering, reflection, and instrumental errors eventually completely swamp out any small absorption, we use the EQE spectra of the samples to measure α in this low absorption region. To do this, we measure α from the $\%T$ data at a wavelength where absorption is moderately high, and can be measured reasonably accurately, but at the same time, at long enough wavelength so that the increase in EQE with shorter wavelength is not close to "saturation" (where the gradient of EQE/photon energy starts to drop). In this region, we assume that changes in α with wavelength are linearly proportional to changes in EQE, which can be measured much more accurately and reliably. We have confirmed that this assumption is valid over a low-moderate absorption range by taking α at one point on the $\%T$ spectrum and feeding in the EQE-derived values of α at longer wavelengths, when we obtain a spectrum essentially the same as the original $\%T$ spectrum. We cannot use this test for very low values of absorption, because the values derived from $\%T$ data in this region are, as we already pointed out, not reliable. However, it is not unreasonable to assume that the validity of the EQE-to-α mapping is valid also in this range, although we cannot say this with certainty.

Figure 5 shows such simulated spectra, which we compare with the measured 140 cycles spectrum from Figure 1. Because

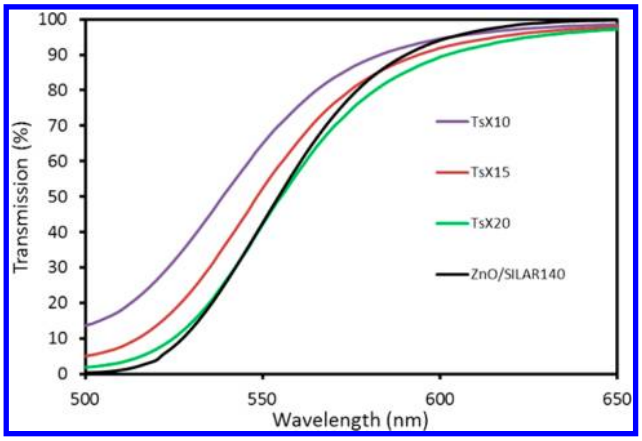

Figure 5. Simulated $\%T$ spectra using absorption coefficients calculated from the planar SILAR film and then multiplying by various multiples ($T_S \times 10$, $T_S \times 15$, $T_S \times 20$) of the local thickness of CdS (from the 140 cycle deposit on ZnO − local thickness 30−33 nm) to obtain $-\ln(T)$ and then T. The multiple ×20 gives the closest fit to the 140 cycles film on ZnO.

we know the local CdS thickness of this sample is 30−33 nm, we can multiply this thickness by some factor that represents the real-to-geometric surface area. From Figure 5, which shows factors of 10, 15, and 20 as well as the 140 cycle from Figure 1, we see that the factor of 20 is closest to the measured 140 cycles on ZnO sample. This then provides a measure of the surface area multiplication of these films. We note that in the long wavelength region, the simulated curve (×20) exhibits stronger absorption than does the measured one. There are a number of possible reasons for this, not least being the inaccuracy in the spectrophotometric readings in this region. What is interesting is that, on the basis of our expectation of multiple scattering in the weakly absorbing spectral region, we should have seen the opposite behavior. This suggests that such multiple scattering does not play an important role in these samples. We stress that the importance of multiple scattering will depend on both the sample morphology and the nature of the illumination. Thus, well-aligned ZnO nanorods and a collimated light source will give much less multiple scattering than nonaligned rods (or nanoparticles) exposed to a high percentage of indirect illumination.

These results strongly suggest that the red shift of the SILAR films is due to an extended, strong sub-bandgap tail in the SILAR films. This would mean that the actual bandgap of the films has not changed, but that there is an effective bandgap lowering in the sense that the films behave as if they had a lower bandgap.

We do not know the specific cause for the strong tailing in the SILAR films, but it is well-known that structural disorder in

dx.doi.org/10.1021/jp3105453 | J. Phys. Chem. C XXXX, XXX, XXX−XXX

semiconductors introduces tailing below the bandgap.[25−28] Some possibilities for such disorder are nonstoichiometry (the films are Cd-rich as discussed later); oxidized surfaces of the small nanocrystals; structural defects; and strain. For CdS powders formed by microwave-assisted hydrolysis of Cd−thiourea complexes, large tails in the absorption were observed that became more prominent with increasing thiourea concentration. It was suggested that the increasing disorder originated from excess S in interstitial sites as S inclusions, either atomic or small aggregates.[29] Such inclusions/aggregates could conceivably form in the SILAR films, even though there is an overall Cd excess. Disorder can localize states near the bandgap (Anderson localization). In this case, the EQE values of solar cells in general are expected to be low due to poor conduction in this spectral region, leading to a blue shift of the EQE spectra as compared to the absorption spectra. This does not occur in our samples, at least for the thinner samples. The EQE of the thinner samples, which are assumed to have the same disorder (unless the disorder is a factor of number of grain boundaries the charge has to pass through, and the CBD samples have a similar number of grain boundaries), is relatively high. The drop in EQE for thicker films can be reasonably explained by increasing recombination through increasing number of crystals as already noted. However, it is also possible that there is another reason for this drop in EQE with increasing thickness.

Tailing into the bandgap in semiconductors is a universal phenomenon. If the tailing occurs due to local electric fields in the semiconductors caused by the defects, whatever their nature, the tail decays exponentially from the band edges into the bandgap. These so-called Urbach tails are characterized by an exponential dependence between α and photon energy given in its simple form by:

$$\alpha \approx \exp(h\nu/E_U)$$

where E_U is a parameter associated with the width of the tail and known as the Urbach parameter. Values of this parameter at room temperature vary from ca. 10−20 meV for high-quality single crystals through many tens of meV for polycrystalline materials and reaching over 0.1 eV for very disordered materials. There have been several reported values of E_U in the literature for as-deposited CBD CdS ranging from 1.35 eV;[30] through 0.22 eV (increasing to >0.8 eV, when defects were introduced by Ar ion implantation and depending on degree of ion damage);[27] 0.094 eV;[31] and down to 0.075 eV (similar to ref 31 but sample annealed at 250 °C in air, which should lower E_U somewhat).[32] It is important to note that the values in refs 27 and 30 were derived from spectrophotometer measurements that were apparently not corrected for reflection losses; this means that the absorption values were probably overestimated. Adding to this is the fact that, as already stressed, measurement of low levels of absorption from spectrophotometer measurements is very imprecise. Therefore, the values in these two references, in particular the extremely high value in ref 30, are suspect. References 31 and 32, on the contrary, used reflection-corrected and photoconductivity response measurements, respectively, which are more likely to be valid.

Figure 6 shows ln(α) versus $h\nu$ plots for the planar CBD and SILAR films on FTO (again, we wanted to minimize complications that might arise from the scattering films on ZnO). The SILAR films shows a wide range of linearity from 2.02 to 2.32 eV. The loss of linearity above 2.32 eV can be explained by crossover into the normal bandgap region. The change in slope below 2.02 eV may reflect a real change in the shape of the tail states at that energy. However, it may also be an artifact caused by errors in the measurement of the small photocurrents in this region, which become increasingly noisy as the wavelength increases, and therefore photocurrent decreases, although this more likely becomes a problem below 1.8 eV (for this particular case). We also measure the Urbach parameter, E_U, to be 0.11 eV, which is a value suggesting a rather high degree of disorder in the CdS. In fact, absorption by this tail dominates the optical spectra of the SILAR films, most clearly seen in the thicker films, in Figure 1. We also note here that SILAR films tend to be nonluminescent (Kamat, P. V., private communication) as may be expected for highly disordered material.

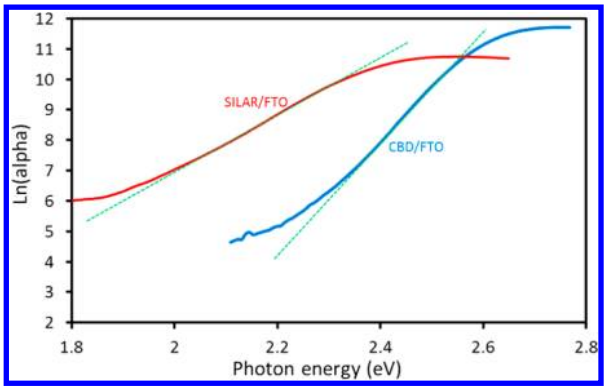

Figure 6. The ln(absorption coefficient) versus $h\nu$ plots for the planar CBD and SILAR films on FTO.

For the CBD sample, the range of linearity is smaller, from 2.35 to 2.54 eV. The bandgap of this size quantized CdS is ca. 2.65 eV (Figure S7, bottom plot), which is in good agreement with a value of ca. 2.6 eV (estimated from Figure. 3) that explains the upper limit as for the SILAR sample. Below 2.2 eV, the photocurrent signal used to measure α becomes too noisy to be very meaningful (α at 2.2 eV is ca. 50 cm^{-1}, which is a very low value). The slope of the CBD spectrum is clearly greater than that for the SILAR sample as can also be seen visually from the high sensitivity EQE tails, giving a value for E_U of 0.05 eV for the CBD sample.

We are still left with an important question: Why is there an apparent red shift as the film becomes thicker? This is not simply a question of greater light absorption due to more material; the difference in the amount of material is not large enough for this explanation to be tenable. For example, the difference in the amount of material between the 50 cycles and 140 cycles samples is, at most, 3 times; yet the absorption of the 140 cycles sample in the low absorption region (e.g., at 2.1 eV) is much greater than three. By the time we have gotten to the 140 cycle sample, however, any further shift (in the 220 sample) can be explained purely by the increasing thickness.

We suggest that the red shift is a balance between two competing effects, one of which is the tail effect we have discussed and the other a size quantization effect. For very thin layers (e.g., 5 cycles), there is a strong blue shift, which is presumably due to size quantization. Vogel et al., in the first demonstration of SILAR-sensitized TiO_2,[3] showed a gradual red shift (both optical and photocurrent spectra) of the CdS/TiO_2 films with increasing number of SILAR cycles and explained the shift, perfectly reasonably, by an increase in CdS crystal size with increasing number of cycles, leading to a

dx.doi.org/10.1021/jp3105453 | J. Phys. Chem. C XXXX, XXX, XXX−XXX

decrease in size quantization of the initially very small CdS crystals. In retrospect, there are signs in that paper of a somewhat anomalously low bandgap for the CdS for 20 and 30 (the maximum) cycle films.

At this point, we return to our Tauc plot data. Despite our reluctance to place too much emphasis on these data, it is worth noting that, for the SILAR films, the apparent direct bandgaps of 2.36−2.38 eV that can be interpreted from the Tauc plots of both the thicker CdS/ZnO films and planar CdS are consistent with our hypothesis that the bandgap of the (thick, nonquantized) SILAR CdS is the normal value of ca. 2.4 eV, but the effective optical absorption over much of the spectral range is dominated by the tail absorption.

Although our TEM images of the 5 cycles sample (XRD showed no pattern for the thinner samples) suggest a crystal size of ca. 4 × 8 nm (likely to be 4 × 4 × 8 nm in 3 dimensions), at which size only a moderate quantum size effect should be seen, the spectrum of the 5 cycle sample is typical of at most 3 nm isotropic CdS particles.[33] It is possible that the actual coherent crystal size was smaller than that measured by TEM, for example, due to some oxidized shell on the crystal surface. In any case, as the film is made thicker and the crystal size increases, as measured by both XRD and TEM for thicker films, the effect of size quantization will become less and the "tail" effect will become dominant.

The CBD sample also seems to show a similar interplay between size quantization and tailing, although the tailing is much less pronounced than in the SILAR samples. The CBD sample on FTO/glass shows a clear blue shift, which is more or less compatible with the crystal size, measured by XRD, of 5 nm (we only can measure one XRD peak, and we have not carried out TEM imaging to see if there is shape anisotropy as occurs with the SILAR films). The same analysis of the CBD film on ZnO gives a crystal size of 6 nm; this may or may not be meaningful. Becauase our emphasis is on the SILAR films and we use the CBD films as a reference, we have not characterized them so fully as the SILAR ones. However, it is clear that the shift in effective bandgap for the CBD films, if it occurs, is much less than for the SILAR films.

The effect of annealing, while only carried out for one sample (140 cycles), is interesting. Annealing shifts the spectrum to the blue (Figures 1 and 2). On the basis of our tailing hypothesis, this can be explained by annealing out of the defects that cause the tailing. It is clear that annealing does not completely remove these defects for two reasons. One, immediately visible, is that the effective bandgap of the annealed sample is still considerably lower than the normal bulk bandgap of CdS (2.4 eV). The second is clear after comparing the shapes of the spectra in the region of low absorption. From the %T spectra (Figure 1), the annealed sample has an even more pronounced tail than the unannealed one. From the EQE spectra (Figure 2), while the overall spectrum of the annealed sample is slightly to the blue of the 100 cycles sample, it crosses over that spectrum at ca. 580 nm and has a larger tail at longer wavelengths (although the tail of the unannealed 140 cycles sample has a much larger amplitude, but not necessarily much greater extension into the red). This means that even after annealing at 540 °C, a considerable, although strongly reduced, amount of the defects that are responsible for the red shift remains.

As we pointed out earlier, in most studies where apparent bandgap narrowing of SILAR films could be deduced, the phenomenon was not explicitly mentioned. There are only two previous papers where it was mentioned and suggestions made as to its cause. Baker and Kamat[6] found a red shift up to ca. 50 nm in the diffuse reflectance spectra of SILAR CdS deposited on TiO_2 nanotubes and nanoparticles, but in the photocurrent spectra, this shift is seen only on the nanotube substrates and little, if at all, on the nanoparticle substrates. They suggest two possible causes for this red shift based on previous related studies.

One is based on an early paper[34] where very thin Cd metal was electrodeposited onto single crystal TiO_2 and then sulfided in a sulfide solution to CdS, and this was repeated. While not SILAR, it can be considered to be related. The authors found a long wavelength tail in the photocurrent spectrum of these samples, and explained the tail by a high degree of disorder on the CdS. While we feel that this explanation is indeed the most likely for the red shift of the SILAR samples, we point out that the photocurrents reported by Gerischer and Lübke in ref 34 are very small and the apparent shift is rather due to a tail (the photocurrents were given on a log scale, which magnifies the importance of the tail) than to a change in effective bandgap.

A second possible cause was suggested on the basis of our own work[35] where nonuniform absorption of different wavelengths of light in semiconductor films, as well as direction of illumination, can lead to differences in the absorption and photocurrent spectral shapes. We feel that this is not a likely explanation in the present case because such effects do not lead to an extension of the spectral range into the red but rather to a masking, to a greater or lesser degree, of the normal red response, which can then be regained under certain conditions.

The red shift was also noted by Ardalan et al.[7] with a reference back to the Baker and Kamat paper[6] repeating the same potential explanations for the phenomenon.

While we believe that the strong tail explanation is the most probable for the red shifts observed for the SILAR films, we consider alternate possible explanations. We can think of three such explanations.

Type II Transition between the CdS Valence Band and ZnO Conduction Band. A type II transition[36,37] between the CdS valence band and ZnO conduction band would seem to be a very reasonable explanation based on the band diagram of CdS on ZnO, which we have measured (by XPS, unpublished) and which would give a type II transition of ca. 2.2 eV that would agree with the red shift we measure experimentally. However, we exclude this possibility because formation of a thick ZnS layer (15 nm) by solution sulfidation of the ZnO before CdS deposition, which should prevent coupling between the CdS valence and ZnO conduction bands, has no effect on the optical spectra. We also note that by its nature, SILAR deposition of sulfides results in formation of a ZnS film on the ZnO, although probably much thinner than that in the above experiment, and it is at least possible that some CdS/ZnO interface could exist.

Another problem with trying to explain our results with a type II transition, even ignoring the ZnS, is that, while electrons excited very close to the CdS/ZnO interface could reasonably be promoted directly to the ZnO conduction band, those excited far from the interface (several nanometers and, even more so, tens of nanometers) are very unlikely to undergo the same transition. Yet it is the thicker CdS films (tens of nanometers) that show the largest red shift.

Surface Effects (Absorption by Surface Species or Effects of the Surface on Band Structure). Surface effects have been shown to change semiconductor nanocrystal effective bandgaps. Chemisorbed molecules, usually organic,

dx.doi.org/10.1021/jp3105453 | J. Phys. Chem. C XXXX, XXX, XXX−XXX

which are themselves often colorless, have been shown to form charge-transfer complexes with very small (several nanometers) TiO_2 particles, resulting in coloration of the particles extending over the visible spectrum depending on the nature of the molecule.[38] Adsorption of certain species or monolayers at semiconductor quantum dot surfaces has resulted in spectral shifts of light absorption, either to the blue or to the red, due to electric field effects.[39−41] Shifts, again to the red or to the blue, due to surface ligand modification have been ascribed to possible structural rearrangements of very small semiconductor nanoparticles (actually more like clusters with diameters of ca. 1.5 nm).[42,43] In all of these cases, the semiconductors involved are in the form of small nanocrystals. Most were at the interface between clusters and nanoparticles, although the CdSe quantum dots reported by Sarkar and Hodes in ref 40 showed clear (blue, not red) shifts over the entire range of size quantization, increasing up to 0.25 eV for quantum dot sizes below 4 nm.

It is very unlikely that any of these surface effects play an appreciable role in the present case for two reasons. One is that they all require appreciable amounts of surface adsorbed species, and such species, if present at all, would exist as impurities at very low concentration levels. Also, according to XRD and TEM results, the CdS crystal size (for the thicker CdS layers, which are more relevant for this discussion) is larger than any of the above cases where red shifts were obtained.

Cd−Cd Bonds in a Cd-Rich CdS As Suggested by Tong et al. in Reference 8. The change in optical properties ascribed to Cd−Cd bonding in Cd-rich CdS in ref 8 is intriguing, particularly as it is probably not an explanation that would immediately spring to mind for anyone not familiar with this reference. The CdS in this study is in the form of nanorods or nanocages built up from CdS nanoparticles with estimated E_g as low as 2.18 eV (from the bulk E_g of ca. 2.4 eV). The rationale for this lowering of E_g was based upon the high Cd excess found in these samples, both nanorods and isolated nanoparticles (Cd:S = 1.17). It was suggested that bonding between interfacial Cd cations on adjacent nanoparticles resulted in hybridization of the Cd cation levels to give new levels inside the (original) bandgap, which were responsible for the lower energy transition: that is, instead of a S3p−Cd5s valence band-conduction band, which is the usual bandgap of CdS, the lowered bandgap is a Cd5s bonding−antibonding transition. This idea appeared to be supported by XPS differences in the Cd peaks between the (red-shifted) nanorods and (blue-shifted, size quantized CdS made up of similar but isolated nanoparticles), as well as by theoretical calculations. A similar, and even larger, bandgap lowering was found by the same group for assembled TiO_2 nanoparticles, and explained in the same general manner.[9]

We note that aggregation of quantum dots has been shown in the past to result in bandgap lowering (ref 40 and references therein). However, these effects are all due to reduction of size quantization upon aggregation, and the bandgap never falls below the normal bulk value, in sharp contrast to the examples in refs 8 and 9 and in this Article.

While we do not completely exclude interaction between surface cations on physically contacting nanoparticles as an explanation of the E_g lowering, as suggested in ref 8, for our SILAR CdS, there are some major differences between our SILAR samples and the samples in ref 8 that cast considerable doubt on this explanation in our case.

One is the issue of Cd excess. In general, we do find Cd excess in our solution deposited CdS, both SILAR and CBD. In fact, the CBD CdS (which does not show the large bandgap lowering, although there is a small tailing effect), even though the crystal size is comparable to that of SILAR CdS, has, on average, a larger Cd excess (Cd:S, measured by XPS, for CBD CdS is typically 1.25, while for SILAR, this would be a particularly high value, and we have measured values as low as just slightly greater than unity). Of particular importance, treatment of a specific SILAR film made by first dipping in S^{2-} then, after rinsing, in Cd^{2+} gave a ratio (measured by XPS) of 1.149. After this same film was dipped in S^{2-}, the ratio fell to 1.006 without any change in the red-shifted spectrum. The ratio measured by EDS (which is not surface sensitive) was the same (Cd:S typically ca. 1.1) both before and after S^{2-} treatment, showing that the effect of the treatment was limited to the nanocrystal surface. However, because the Cd−Cd bonding suggested in ref 8 is also limited to the surface, we would expect this bond to be affected by the S^{2-} treatment, and this does not appear to be the case.

The other major difference is that we do not find the differences in the Cd XPS peaks between SILAR CdS and our CBD CdS. At the same time, we must raise a reservation we have with the XPS results in ref 8: The Cd3d XPS peaks normally do not show large chemical shifts, but the Cd3d peaks of the red-shifted CdS in ref 8 are increased by ca. 1.5 eV, together with a very large broadening that suggests that charging may be playing a dominant role in that case. For this reason, we consider this difference in the XPS spectra of lesser importance than the previous issue of (non)stoichiometry and the possible resulting Cd−Cd bonding.

To sum, while we consider the extended tail states hypothesis to be a more straightforward and likely explanation for the red shifts seen in the SILAR films, we do not completely reject the idea of Cd−Cd bonding to explain (or partly explain) our observations.

We consider the importance of this red shift. As we already noted, in contrast to many papers showing red-shifted absorption but poor photocurrent response, SILAR (and also the aggregated nanoparticle structures of ref 8) has been shown, both in a number of previous studies (in many cases not explicitly) as well as the present one, to give moderately good photoresponse with reasonable values of quantum efficiency, which, however, do drop as the local film thickness increases, that is, the effective bandgap decreases. Thus, the red shift observed in optical measurements is also reflected in their solar cell behavior. In terms of an effective bandgap that describes the actual photocurrent response, a reduction of ca. 10% can be obtained for CdS. This is a useful fraction, which increases the range of semiconductors as does size quantization, but in the opposite direction (if to a lesser degree, at least at present). With regard to the drop in EQE as the film thickness increases, it is possible that this can be substantially mitigated by a suitable passivation treatment. Such a treatment, coating with two cycles of SILAR ZnS, is well-known for CdSe absorbers in SSSCs.[44] However, in our hands, this treatment has no effect on CdS absorbers, even when the CdS is deposited by different methods.

Finally, we return to the difference in absorption coefficients of the SILAR and CBD CdS. From Figure 3, for the films on FTO/glass, we can calculate α for the two films at the wavelengths just blue of the knee, after the steep drop in %T, where the change in absorption (transmission) becomes more

dx.doi.org/10.1021/jp3105453 | J. Phys. Chem. C XXXX, XXX, XXX−XXX

gradual and the absorption is relatively high. For the 70 nm SILAR sample, $\alpha = 1.2 \times 10^5$/cm, while for the CBD sample, $\alpha = 7.3 \times 10^4$/cm. The latter is typical for CdS, where literature values of α begin to level off at ca. 8×10^4/cm; the value for the SILAR CdS at the equivalent position on its spectrum is nearly twice as high as that of the CBD sample. Besides being favorable for photovoltaic purposes, because thinner layers are needed, the high absorption coefficient implies that the disorder causing the tailing originates from bulk defects rather than (or at least in addition to) surface and interface defects because the density of the defect levels is clearly very high.

CONCLUSIONS

We have investigated the red shift (up to ca. 0.25 eV) in the optical spectra of SILAR CdS deposited on ZnO nanorods. We suggest that the red shift is due not to a change in bandgap of the CdS layer but rather to a pronounced sub-bandgap tailing, which is amplified by the high surface area in the composite CdS/ZnO film. In comparison, chemical bath deposited CdS on ZnO exhibits a much smaller red shift. We also considered other possible explanations for the red shift (type 2 transition; surface absorption; hybridization of Cd−Cd bonds between adjacent nanocrystals): we present strong evidence against the first two options and weaker evidence against the third. While we do not know at this stage the origin of the pronounced tailing, if it could be engineered into other materials, this could present a more general method of extending the effective spectral response of semiconductors to longer wavelengths. In addition, the absorption coefficient of the SILAR CdS is substantially higher than normal, meaning thinner layers are needed to absorb light. The combination of anomalously high absorption coefficient and very small local thicknesses (often below 10 nm) can explain why SILAR CdS (and probably CdSe) works so well in semiconductor-sensitized nanoporous cells, even though the semiconductor quality is rather poor, as seen by the drop in quantum efficiency with increasing thickness. Thus, SILAR absorbers are a good example of the assumed main justification of these nanoporous cells, that poorer quality absorbers can be used as compared to other types of cells.

ASSOCIATED CONTENT

Supporting Information

TEM images of CdS/ZnO. Bandgap analysis plots for nanoporous and flat films. High sensitivity quantum efficiency spectra of tails. Correlation of spectra with light scattering/optical absorber thickness. SEM cross-section images of variable thickness samples. This material is available free of charge via the Internet at http://pubs.acs.org.

AUTHOR INFORMATION

Corresponding Author

*E-mail: gary.hodes@weizmann.ac.il.

Notes

The authors declare no competing financial interest.

ACKNOWLEDGMENTS

We thank Nir Klein-Kedem for carrying out the TEM imaging. We acknowledge the Israel Ministry of Science (Tashtiot programme) and the Harold Perlman family's historic generosity.

REFERENCES

(1) Nicolau, Y. *Appl. Surf. Sci.* **1985**, *22*−*23*, 1061−1074.
(2) Ristov, M.; Sinadinovski, G.; Grozdanov, I. *Thin Solid Films* **1985**, *123*, 63−67.
(3) Vogel, R.; Pohl, K.; Weller, H. *Chem. Phys. Lett.* **1990**, *174*, 241−246.
(4) Vogel; Hoyer, P.; Weller, H. *J. Phys. Chem.* **1994**, *98*, 3183−3188.
(5) Kamat, P. V.; Tvrdy, K.; Baker, D. R.; Radich, J. G. *Chem. Rev.* **2010**, *110*, 6664−6688.
(6) Baker, D. R.; Kamat, P. V. *Adv. Funct. Mater.* **2009**, *19*, 805−811.
(7) Ardalan, P.; Brennan, T. P.; Lee, H.-B.-R.; Bakke, J. R.; Ding, I.-K.; McGehee, M. D.; Bent, S. F. *ACS Nano* **2011**, *5*, 1495−1504.
(8) Tong, H.; Umezawa, N.; Ye, J.; Ohno, T. *Energy Environ. Sci.* **2011**, *4*, 1684−1689.
(9) Tong, H.; Umezawa, N.; Ye, J. *Chem. Commun.* **2011**, *47*, 4219.
(10) Kokotov, M.; Hodes, G. *J. Mater. Chem.* **2009**, *19*, 3847−3854.
(11) Ortuño López, M. B.; Valenzuela-Jáuregui, J. J.; Sotelo-Lerma, M.; Mendoza-Galván, A.; Ramírez-Bon, R. *Thin Solid Films* **2003**, *429*, 34−39.
(12) Edri, E.; Rabinovich, E.; Niitsoo, O.; Cohen, H.; Bendikov, T.; Hodes, G. *J. Phys. Chem. C* **2010**, *114*, 13092−13097.
(13) Smith, G. B.; Ignatiev, A.; Zajac, G. *J. Appl. Phys.* **1980**, *51*, 4186−4196.
(14) Mastai, Y.; Hodes, G. *J. Phys. Chem.* **1997**, *101*, 2685−2690.
(15) Gal, D.; Hodes, G. *J. Electrochem. Soc.* **2000**, *147*, 1825−1828.
(16) Tak, Y.; Hong, S. J.; Lee, J. S.; Yong, K. *J. Mater. Chem.* **2009**, *19*, 5945−5951.
(17) Seol, M.; Kim, H.; Tak, Y.; Yong, K. *Chem. Commun.* **2010**, *46*, 5521.
(18) Woo Jung, S.; Kim, J.-H.; Kim, H.; Choi, C.-J.; Ahn, K.-S. *J. Appl. Phys.* **2011**, *110*, 044313.
(19) Hodes, G. *J. Phys. Chem. C* **2008**, *112*, 17778−17787.
(20) Gärtner, W. W. *Phys. Rev.* **1959**, *116*, 84−87.
(21) Wang, Y.; Hao, Y.; Cheng, H.; Ma, J.; Xu, B.; Li, W.; Cai, S. *J. Mater. Sci.* **1999**, *34*, 2773−2779.
(22) Nakamura, R.; Tanaka, T.; Nakato, Y. *J. Phys. Chem. B* **2004**, *108*, 10617−10620.
(23) Chen, X.; Liu, L.; Yu, P. Y.; Mao, S. S. *Science* **2011**, *331*, 746−750.
(24) Jaramillo, T. F.; Baeck, S.-H.; Kleiman-Shwarsctein, A.; Choi, K.-S.; Stucky, G. D.; McFarland, E. W. *J. Comb. Chem.* **2005**, *7*, 264−271.
(25) Cody, G. D.; Tiedje, T.; Abeles, B.; Moustakas, T. D.; Brooks, B.; Goldstein, Y. *J. Phys. (Paris)* **1981**, *42*, 301−304.
(26) Arendse, C. J.; Malgas, G. F.; Muller, T. F. G.; Heerden, B. A.; Knoesen, D. *J. Mater. Sci.* **2009**, *44*, 6333−6337.
(27) Narayanan, K. L.; Vijayakumar, K. P.; Nair, K. G. M.; Thampi, N. S. *Physica B* **1997**, *240*, 8−12.
(28) Parmar, M. N.; Patel, C. D.; Kulshrestha, A. *J. Adv. Eng. Tech.* **2012**, *3*, 208−212.
(29) Podborska, A.; Gaweł, B.; Pietrzak, Ł.; Szymańska, I. B.; Jeszka, J. K.; Łasocha, W.; Szaciłowski, K. *J. Phys. Chem. C* **2009**, *113*, 6774−6784.
(30) Rizwan, Z.; Zakaria, A.; Mohd Ghazali, M. S.; Jafari, A.; Din, F. U.; Zamiri, R. *Int. J. Mol. Sci.* **2011**, *12*, 1293−1305.
(31) Rakhshani, A. E.; Al-Azab, A. S. *J. Phys.: Condens. Matter* **2000**, *12*, 8745−8755.
(32) Rakhshani, A. E. *J. Phys.: Condens. Matter* **2000**, *12*, 4391−4400.
(33) Sapra, S.; Sarma, D. D. *Phys. Rev. B* **2004**, *69*, 125304.
(34) Gerischer, H.; Lübke, M. *J. Electroanal. Chem.* **1986**, *204*, 225−227.
(35) Hodes, G.; Howell, I. D. J.; Peter, L. M. *J. Electrochem. Soc.* **1992**, *139*, 3136−3140.
(36) Kim, S.; Fisher, B.; Eisler, H.-J.; Bawendi, M. *J. Am. Chem. Soc.* **2003**, *125*, 11466−11467.
(37) Ning, Z.; Tian, H.; Yuan, C.; Fu, Y.; Qin, H.; Sun, L.; Ågren, H. *Chem. Commun.* **2011**, *47*, 1536−1538.
(38) Rajh, T.; Chen, L. X.; Lukas, K.; Liu, T.; Thurnauer, M. C.; Tiede, D. M. *J. Phys. Chem. B* **2002**, *106*, 10543−10552.

(39) Sarkar, S. K.; Chandrasekharan, N.; Gorer, S.; Hodes, G. *Appl. Phys. Lett.* **2002**, *81*, 5045−5047.
(40) Sarkar, S. K.; Hodes, G. *J. Phys. Chem. B* **2005**, *109*, 7214−7219.
(41) Yaacobi-Gross, N.; Soreni-Harari, M.; Zimin, M.; Kababya, S.; Schmidt, A.; Tessler, N. *Nat. Mater.* **2011**, *10*, 974−979.
(42) Landes, C.; Braun, M.; Burda, C.; El-Sayed, M. A. *Nano Lett.* **2001**, *1*, 667−670.
(43) Cossairt, B. M.; Juhas, P.; Billinge, S. J. L.; Owen, J. S. *J. Phys. Chem. Lett.* **2011**, *2*, 3075−3080.
(44) Diguna, L. J.; Shen, Q.; Kobayashi, J.; Toyoda, T. *Appl. Phys. Lett.* **2007**, *91*, 0231161−3.